

Article

Performance Tradeoff Analysis of Hybrid Signaling SWIPT Systems with Nonlinear Power Amplifiers

Linlin Chen ¹, Xiaofang Wu ^{1,2,*} , Xin Wang ¹, Wen Qi ^{1,2} , Xuemin Hong ¹, Jianghong Shi ¹, Jie Hu ³ and Kun Yang ³

¹ National-Local Joint Engineering Research Center of Navigation and Location Services, Xiamen University, Xiamen 361000, China; 23320181154359@stu.xmu.edu.cn (L.C.); wx11220831@126.com (X.W.); 23120201150239@stu.xmu.edu.cn (W.Q.); xuemin.hong@xmu.edu.cn (X.H.); shijh@xmu.edu.cn (J.S.)

² School of Electronic Science and Engineering, Xiamen University, Xiamen 361000, China

³ School of Information and Communication Engineering, University of Electronic Science and Technology of China, Chengdu 611731, China; hujie@uestc.edu.cn (J.H.); kunyang@uestc.edu.cn (K.Y.)

* Correspondence: xfwu@xmu.edu.cn

Abstract: Simultaneous wireless information and power transfer (SWIPT) is a promising technology to achieve wide-area energy transfer by sharing the same radio frequency (RF) signal and infrastructure of legacy wireless communication systems. To enlarge the effective range of energy transfer in practice, it is desirable to have a hybrid signaling SWIPT scheme, which combines a high-power multitone energy signal with a low-power broadband information signal. This paper presents a systematic study on the performance of hybrid signaling SWIPT systems with memoryless nonlinear transmitter power amplifiers (PAs). Using PA efficiency and signal-to-noise-and-distortion ratio (SNDR) as the metrics to measure the efficiency of energy transfer and information transmission, respectively, we derive the tradeoff between these two metrics for two PA classes, two nonlinear PA models, and two SNDR definitions. Our results reveal insights into the fundamental performance tradeoff inherent in SWIPT systems using hybrid signaling schemes.

Keywords: SWIPT; SNDR; energy conversion efficiency; nonlinear PA



Citation: Chen, L.; Wu, X.; Wang, X.; Qi, W.; Hong, X.; Shi, J.; Hu, J.; Yang, K. Performance Tradeoff Analysis of Hybrid Signaling SWIPT Systems with Nonlinear Power Amplifiers.

Electronics **2021**, *10*, 1364.
<https://doi.org/10.3390/electronics10111364>

Academic Editor: Athanasios Kanas

Received: 30 April 2021

Accepted: 1 June 2021

Published: 7 June 2021

Publisher's Note: MDPI stays neutral with regard to jurisdictional claims in published maps and institutional affiliations.



Copyright: © 2021 by the authors. Licensee MDPI, Basel, Switzerland. This article is an open access article distributed under the terms and conditions of the Creative Commons Attribution (CC BY) license (<https://creativecommons.org/licenses/by/4.0/>).

1. Introduction

Along with the rapid commercialization of the 5th generation (5G) mobile communication technology, research and development of the 6th generation (6G) network is gaining momentum [1]. Enabled by 5G and 6G technologies, Internet of things (IoT) is quickly becoming ubiquitous in people's daily lives. A key challenge hindering the proliferation of IoT is to provide power-deficient sensor devices with a reliable and sustainable energy supply [2]. Conventional energy supply technologies, such as wired charging [3], near-field wireless charging [4], and renewable energy harvesting (EH) [5], are limited by either the short distance or the availability of energy sources; hence, their applicability is constrained to specific scenarios. Exploiting the fact that radio signals are widely used for modern wireless communication systems, radio frequency energy transfer (RFET) technology was proposed as a ubiquitous energy supply technology that can continuously harvest the weak energy of far-field radio signals from the environment [6]. Simultaneous wireless information and power transfer (SWIPT) systems [7] take a step further to propose that concurrent information transmission and energy transfer can be integrated into a single system and jointly optimized at both the signaling and device levels.

In a typical SWIPT scenario, information and energy transmitters share the same transmitting device, whereas receivers for energy harvesting (EH) and information decoding (ID) are not necessarily co-located. Based on whether the EH and ID receivers are co-located, SWIPT systems have two operational models: standalone and co-located models. The former uses separated antennas on different devices for EH and ID, respectively, as shown in Figure 1a. The latter has one device for signal reception and needs to

separate the analog signal received by the antenna (or antenna array) into two signals by means of time division [8–10], power division [11–14], space division [15–17], or frequency-splitting [18]. The separated signals are then fed into the ID receiver and EH receiver, respectively, as shown in Figure 1b. The potential benefits of SWIPT systems include improved spectrum utilization, reduced overall energy consumption, and reduced cost with shared infrastructure. Nevertheless, significant challenges remain in SWIPT systems to balance the conflicting goals of information transmission and energy transfer and ensure the coexistence of the two systems [19–21].

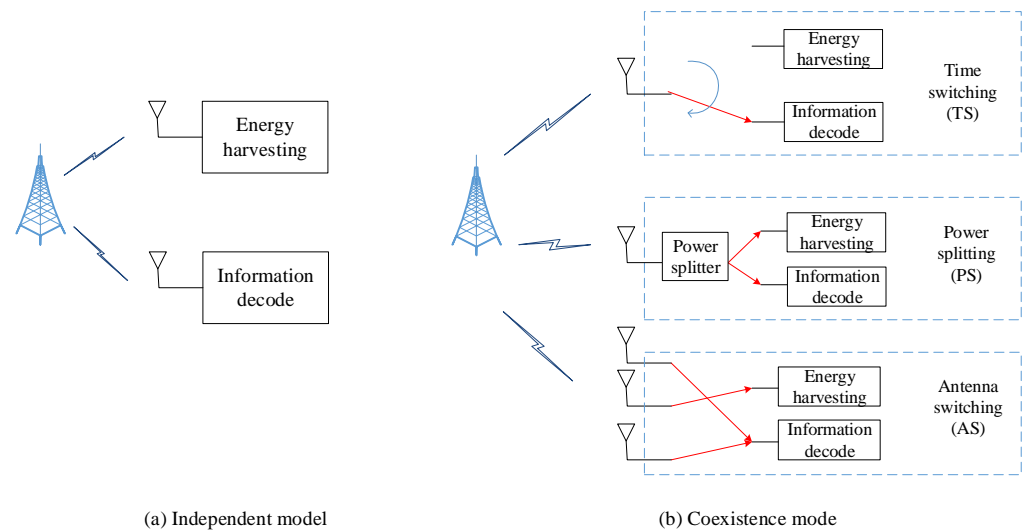


Figure 1. Illustration of SWIPT systems in independent and coexistence modes.

As a potentially disruptive technology, SWIPT has attracted significant research attention in recent years. Papers [22–24] analyzed the trade-off between the spectrum efficiency and energy efficiency of information transmission from the perspective of information theory. The authors in [25–27] studied the optimization of coding, modulation, and resource allocation. The problem of optimal power allocation in wireless propagation channels under transmit power constraints was investigated in [28,29]. Paper [30] studied the issue of receiver operation and dynamic power allocation. Paper [31] exploited the non-orthogonal-multiple-access (NOMA) technique and proposed a transmit power allocation scheme to improve the spectrum efficiency of a SWIPT system. A comprehensive survey of recent advances in SWIPT systems was given in [32]. The nonlinear model of energy harvesting is also an important research topic for SWIPT systems [20]. Paper [33–35] studied the intelligent reflecting surface (IRS) system and investigated how to use IRS to improve the energy collection efficiency of a SWIPT system. In order to highlight the tradeoff between SNDR and PA efficiency, the above discussion focused on the transmitter side with the basic single-input-single-output (SISO) hybrid signal. When extended to the whole SWIPT system, there remain many important and need research areas, such as energy harvesting circuit, signal modulation, multiple-input-multiple-output (MIMO), energy waveform design, and multipath channel estimation [19–21]. A research area that requires immediate attention is how to enhance the power efficiency of the total SWIPT system, which is a combination of the PA DC-to-RF conversion efficiency, RF-to-RF transmission efficiency, and the energy harvesting circuit RF-to-DC conversion efficiency. Especially when the signal power is low, the efficiencies are coupled with each other due to the nonlinearity of the energy harvester circuit [19]. Another promising area is the MIMO-OFDM modulation scheme; the use of multi-antenna beamforming can further increase the DC power of the energy harvesting circuit. However, it is more sensitive to the nonlinear distortion of PA, especially the phase distortion, and more efforts are needed to estimate the dynamic nature of a MIMO channel [21]. For the whole SWIPT system, more performance metrics at the

receiver side are needed to evaluate the efficiency of information transmission, such as signal-to-interference-plus-noise ratio (SINR) and bit-error-rate (BER). This also leads to interesting new challenges in terms of the information rate and delivered energy trade-off for the whole system. These works, along with the majority of theoretical SWIPT studies in the literature, imply an idealized assumption that energy receivers can effectively harvest radio signals of arbitrary power strength. However, in practice, due to the physical characteristics of electronic devices, RF energy harvesting is only feasible when the received signal strength is above a certain threshold. Compared with ID receivers that typically work at a signal strength of around -90 dBm [36], EH receivers require a much higher signal strength of around -40 dBm to function properly [37]. Such a drastic difference should be taken into account during the design of SWIPT signaling schemes.

Two types of SWIPT signaling schemes have been proposed in the literature: identical signaling schemes and hybrid signaling schemes. The former uses a common transmit signal for EH and ID, as illustrated in Figure 2a. The advantage of this scheme is that it encourages the maximum reuse of existing information signals transmitted by legacy wireless communication systems. However, as wireless communications systems are designed for high spectrum utilization, tight transmit power constraints are imposed on information-bearing wideband RF signals. As a result, the effective range of energy transfer in a SWIPT system with identical signaling would be very short; hence, this system has limited practical value.

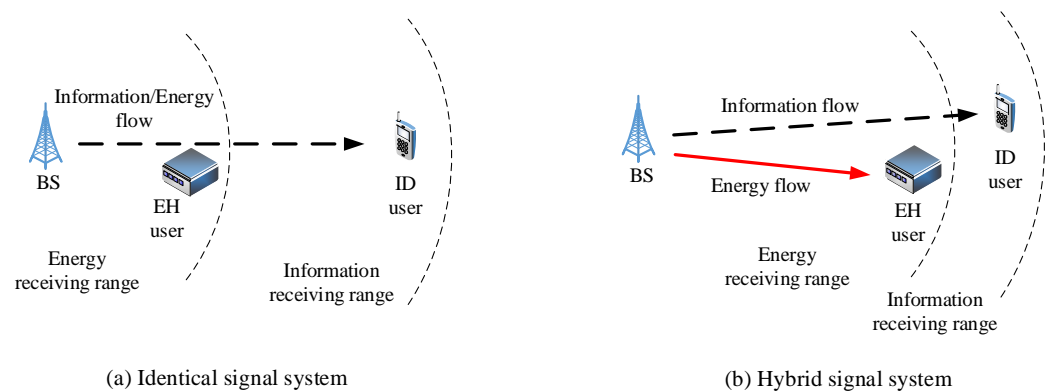


Figure 2. Illustration of SWIPT systems with identical and hybrid signaling schemes.

To overcome the drawback of identical signaling, a hybrid signaling scheme has been proposed [38], as shown in Figure 2b. It consists of a low-power broadband information signal and a high-power, small-bandwidth energy signal [39]. The energy signal is typically an unmodulated multitone sinusoid signal, whose signal waveform can be optimized to improve the energy harvesting efficiency by increasing the peak-to-average power ratio (PAPR) [40–43]. To date, reported research on hybrid signaling SWIPT has covered multiple topics, including the topics of beamforming and optimal power allocation [44,45], the tradeoff between information transmission and energy transfer [46], and the impacts of baseband modulation on the efficiency of energy and data transmission [41].

In the existing SWIPT research literature, most studies have focused on the receiver side, while assuming that the transmitter performs ideal linear amplification on the signal. Receiver-side nonlinearity has also been studied in energy harvesting schemes for multiple applications such as IoT [47]. On the contrary, transmitter-side nonlinearity is still under-investigated. In practice, the high-power energy signal transmission may drive the transmit PA to work on the nonlinear region and cause serious interference with the information signal. Although there exists a wealth of conventional studies that investigate nonlinear transmit PA in communication systems, the signaling schemes in these studies are restricted to pure information signals. In the HSS-SWIPT system considered in this paper, the transmitted signal is a mixture of a high-power energy signal and low-power information signal. Nonlinear amplification will result in spectrum spreading of the in-

formation signal. Furthermore, the two signals will produce intermodulation distortion, which will further degrade the information signal quality. On one hand, for high-power energy signals, we prefer the PA to work in the nonlinear region to improve the energy conversion efficiency; on the other hand, for low-power information signals, nonlinear distortions of the signal should be avoided as far as possible [48,49]. As a result, achieving high efficiency of energy conversion and low distortion of the information signal become conflicting objectives. As nonlinear PA is practically unavoidable, it is of great importance to investigate the tradeoff between energy transfer and information transmission in a hybrid signaling SWIPT [50].

This paper is among the first efforts to analyze the performance of hybrid signaling SWIPT systems with nonlinear PA. Because nonlinear PA is a transmitter-side phenomenon, we restrict our study to performance metrics at the transmitter side. In other words, receiver-side particularities such as modulation and circuit designs are deliberately made irrelevant and neglected. This helps us to decouple the problem and obtain deeper insights. More specifically, we use the transmitter-side signal-to-noise-and-distortion ratio (SNDR) [51,52] to measure the efficiency of information transmission, and the transmitter PA efficiency to measure the efficiency of energy transfer. This paper makes the following contributions: first, the SNDR metrics are redefined for the SWIPT system with hybrid signaling, which consists of a high-power energy signal and a small-power information signal; second, the SNDR and the PA efficiency are analytically evaluated for SWIPT systems with nonlinear PAs; finally, using the input back-off (IBO) as the intermediate parameter, we quantify the tradeoff between the SNDR and the PA efficiency.

The remainder of this paper is organized as follows. Section 2 introduces the system model and presents definitions of the performance metrics. Theoretical evaluations of PA energy conversion efficiency and information signal SNDR are presented in Sections 3 and 4, respectively. Section 5 analyzes the tradeoff relationship between PA efficiency and SNDR in hybrid signaling SWIPT systems. Finally, conclusions are drawn in Section 6.

2. System Model

Figure 3 shows the system model of the hybrid signaling SWIPT system studied in this paper. We assumed that the information signal $s(t)$ uses an orthogonal frequency division multiplexing (OFDM) signal and the energy signal $e(t)$ uses a multitone sine signal [41]. Mathematically, these two signals are defined as

$$s(t) = \sum_{k=0}^{K-1} B_k(t) \exp(j(2\pi f_k t + \phi_k)), \quad (1)$$

$$e(t) = \sum_{n=-N}^N D_n \exp\left(j\left(2\pi\left(f_n + n\Delta_f\right)t + \phi_n\right)\right) \quad (2)$$

where $B_k(t)$ is the baseband waveform signal, D_n is the amplitude of the sinusoid signal at each frequency point, f_k and ϕ_k denote the frequency and initial phase of the OFDM subcarrier, respectively, f_n and ϕ_n denote the center frequency and initial phase of the sinusoid signal, respectively, and Δ_f is the frequency offset of the multitone sine signal.

The two signals are superimposed and fed into a PA before transmission into a wireless channel. The receiver uses power splitting to separate the received signal into the information signal and energy signal, which are subsequently used for ID and EH, respectively. As mentioned above, the focus of our paper is on the nonlinear distortion at the transmitter side caused by the PA. Common RF PAs can be classified into two categories: memoryless PA and PA with memory. In a memoryless PA, the output is an instantaneous function of the input. Therefore, any change in the input signal results in instantaneous reactions at the output. In contrast, in a PA with memory, the output is also a function of previous input values. Our paper focuses on the case of memoryless PA, leaving the more complicated case of PA with memory as future work. The signal distortion and power

efficiency of a PA depend on its nonlinear distortion model and input power back-off (IBO). The PA models and the concept of IBO will be subsequently introduced as preliminaries.

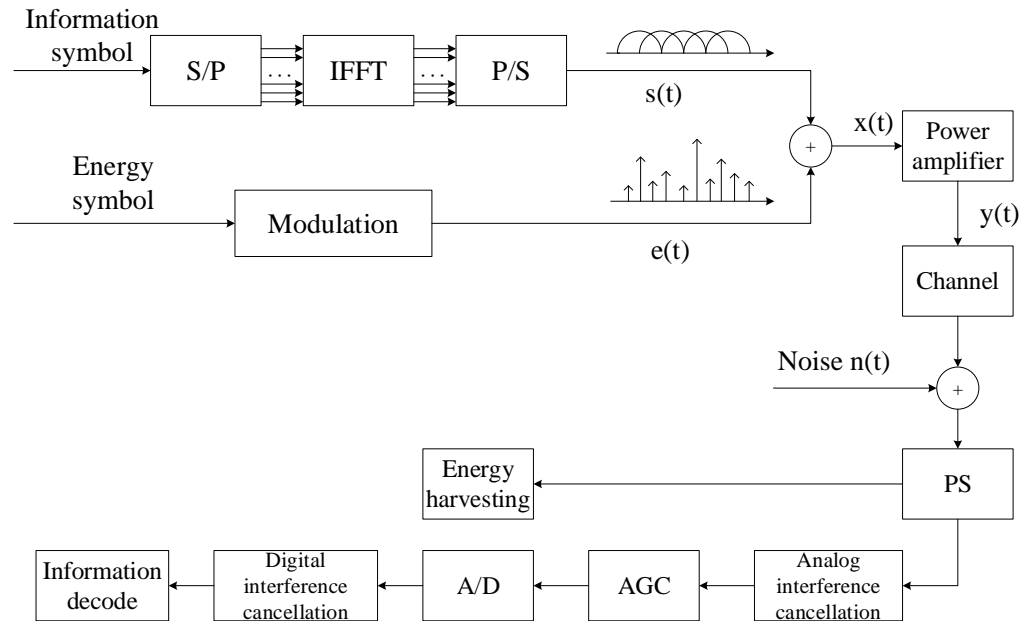


Figure 3. System model.

2.1. Memoryless Nonlinear PA Models

As illustrated in the system model in Figure 3, the complex baseband information signal can be written as $s(t) = r_s(t) \exp(j\phi_s(t))$. Similarly, the complex baseband energy signal can be written as $e(t) = r_e(t) \exp(j\phi_e(t))$. It follows that the total complex baseband input signal, which is obtained by the superposition of the information signal and energy signal, is given by $x(t) = s(t) + e(t) = r(t) \exp(j\phi(t))$. The output signal $y(t) = r_o(t) \exp(j\phi_o(t))$ is the complex baseband output signal of the nonlinear PA. For the memoryless PA, the output signal $y(t)$ can be regarded as a function of the envelope of the input signal $r(t)$, i.e.,

$$y(t) = g(r(t)) \exp(j(\phi(t) + f(r(t)))) \tag{3}$$

where $g(r(t))$ and $f(r(t))$ are the magnitude response and phase response of $r(t)$, respectively. The magnitude response and phase response are commonly referred to as AM-AM and AM-PM characteristics. Because the time variable t is not important in a memoryless PA model, it will be neglected in the remainder of this paper for clarity.

2.1.1. Ideal Linear PA Model

For comparison purposes, we first introduce an ideal linear PA model. In such a model, the amplifier has no phase distortion, i.e., we have $f(r) = 0$ for any r . The AM-AM characteristic of the linear PA model can be expressed as [46]

$$g(r) = \begin{cases} r_{o,max} \left(\frac{r}{r_{max}} \right), & r < r_{max}, \\ r_{o,max}, & r \geq r_{max}, \end{cases} \tag{4}$$

where $r_{o,max}$ is the maximum output signal envelope and r_{max} is the maximum input signal envelope for linear amplification input. These two variables are related by

$$r_{o,max} = Ar_{max} \tag{5}$$

where A represents the constant amplitude (envelope) gain of the idealized PA. The characteristics of this ideal model can be used as a reference benchmark for other nonlinear PA models [53].

2.1.2. Saleh Model

The Saleh model was first obtained by statistical analysis of the input and output data of travelling-wave tube amplifiers (TWTA) [54]. It has a simple structure, but can describe the nonlinear characteristics of TWTA accurately. The model also has high fitting performance for the measured data of other memoryless PAs. Therefore, it is widely used as a memoryless PA model in modern communication systems [55].

Our paper adopts a normalized Saleh PA model, whose AM-AM and AM-PM characteristics are given by

$$g(r) = \frac{a_1 \frac{r}{r_{\max}}}{1 + b_1 \left(\frac{r}{r_{\max}}\right)^2}, \tag{6}$$

$$f(r) = \frac{a_2 \left(\frac{r}{r_{\max}}\right)^2}{1 + b_2 \left(\frac{r}{r_{\max}}\right)^2} \tag{7}$$

respectively. Without loss of generality, the values of model parameters are taken from numerical values reported in [52]. Specifically, we have $a_1 = r_{o,\max}$, $b_1 = 1/4$, $a_2 = \pi/12$, and $b_2 = 1/4$.

2.1.3. Memoryless Polynomial Model

The memoryless model based on polynomial equations is essentially the complex baseband form of Taylor series used in the analysis of memoryless nonlinear systems. Considering that the band-pass signal after the PA only retains the signal near the central frequency, other frequency components will be filtered out. Thus, only odd-order nonlinear terms should be retained. The mathematical expression of the memoryless polynomial model is given by [56]

$$y(t) = \sum_{k=0}^K a_{2k+1} |x(t)|^{2k} x(t). \tag{8}$$

The polynomial model has wider applicability than the Saleh model and can be used to fit most memoryless RF PAs. When the model coefficients a_{2k+1} are complex-valued, the system is called a quasi-memoryless system, in which the AM-PM characteristic will change with $|x(t)|$. When the coefficients are real numbers, the system is called a strictly memoryless system, such that the AM-PM characteristic is constant at 0, i.e., there is no phase distortion. To facilitate theoretical analysis, this paper adapts a strict memoryless PA model with a small nonlinear order ($K = 2$). After normalizing the polynomial model, we obtain

$$y = r_{o,\max} \left(\frac{x}{r_{\max}}\right) + c_1 r_{o,\max} \left|\frac{x}{r_{\max}}\right|^2 \left(\frac{x}{r_{\max}}\right) + c_2 r_{o,\max} \left|\frac{x}{r_{\max}}\right|^4 \left(\frac{x}{r_{\max}}\right). \tag{9}$$

According to the normalized limit criterion of the ideal linear model, the model coefficients can be calculated to obtain $c_1 = -3/16$ and $c_2 = 1/64$. The detailed derivation process is given in Appendix A. The AM-AM characteristics of the polynomial model can then be written as

$$g(r) = r_{o,\max} \frac{r}{r_{\max}} + c_1 r_{o,\max} \left(\frac{r}{r_{\max}}\right)^3 + c_2 r_{o,\max} \left(\frac{r}{r_{\max}}\right)^5. \tag{10}$$

Because the coefficients of the model are all real numbers, there is no AM-PM distortion, i.e., $f(r) = 0$.

2.2. Input Power Back-Off

Figure 4 shows the AM-AM characteristics of the three PA models described above. It can be seen that in both the Saleh and polynomial models, when the input signal amplitude is less than r_{\max} , a smaller value of r/r_{\max} leads to a better linear amplification property. The IBO is defined as the ratio of r_{\max}^2 to the average power [53], i.e.,

$$\zeta = \frac{r_{\max}^2}{P_{\text{in}}} \tag{11}$$

where $P_{\text{in}} = E[r^2] = E[|x|^2]$ is the average power of the input signal and $E[\cdot]$ denotes the expectation function.

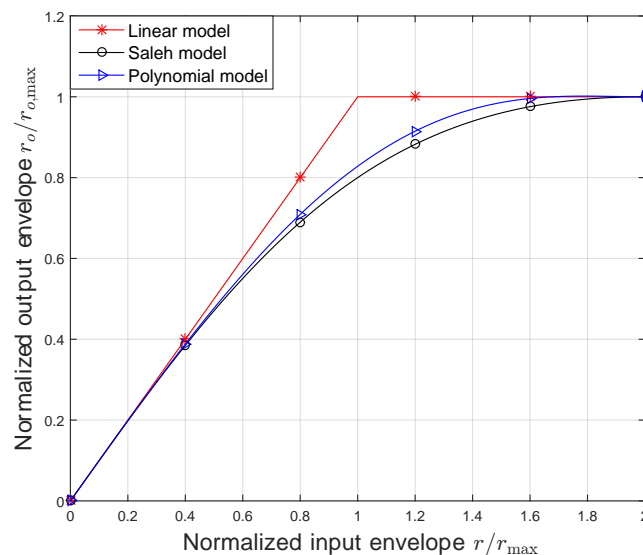


Figure 4. Normalized AM-AM characteristics.

In actual applications, the IBO is usually defined with respect to the 1 dB compression point instead of the maximum limit. This is called effective IBO, which is defined as [53]

$$\zeta_{\text{eff}} = \frac{r_{1\text{dB}}^2}{P_{\text{in}}} = k^2 \zeta \tag{12}$$

where k is the relative 1 dB compression point, and $r_{1\text{dB}} = kr_{\max}$. The 1 dB compression point is defined by the following equation:

$$G_{\text{dB}}(r_{1\text{dB}}) = 10 \lg \left| \frac{g(r)}{Ar} \right|^2 = -1. \tag{13}$$

Based on the above equation, the value of $r_{1\text{dB}}$ can be calculated from the PA's AM-AM characteristic. It follows that the 1 dB compression coefficient k can be obtained as $k = r_{1\text{dB}}/r_{\max}$. For the Saleh model and polynomial model in Figure 4, k is given by 0.6986 [53] and 0.7817, respectively. In the rest of this paper, the term IBO refers to effective IBO.

3. Calculation of PA Efficiency

The average efficiency of PA is defined as the ratio of the average power of the generated RF signal for actual transmission, which is denoted as P_{RF} , and the direct current

(DC) input power supplied by the DC source to the transistor PA circuit, which is denoted as P_{DC} . Both P_{RF} and P_{DC} are functions of the output envelope level r_o . It follows that the average PA efficiency is given by [41,56]:

$$\eta_{av} = \frac{P_{o,av}}{P_{i,av}} = \frac{E[P_{RF}(r_o)]}{E[P_{DC}(r_o)]}. \tag{14}$$

The RF PAs commonly used in communication systems include Class A, Class B, and Class AB types. In recent years, some new PA circuit structures have emerged, such as envelope tracking PAs and Doherty PAs. These new types of PAs can effectively improve the efficiency at the cost of higher nonlinear distortion. In communication systems, the nonlinear distortion in PAs can be corrected by linearization techniques [57–60]. In this paper, we restrict our discussions on classic Class A and Class B PAs, noting that the efficiency of Class AB PAs is between Class A and Class B. The empirical efficiency models for Class A and Class B PAs are presented in [61]. The maximum average efficiency achieved by these two types of PAs can be written as [53]

$$\begin{aligned} \eta_{av,A} &= \frac{1}{2} \frac{E[r_o^2]}{r_{o,max}^2}, \\ \eta_{av,B} &= \frac{\pi}{4} \frac{E[r_o^2]}{r_{o,max} E[r_o]}. \end{aligned} \tag{15}$$

This shows that the efficiency function is the first and second non-central moments of the output signal envelope [53]. Moreover, the standardized n th non-central moment is defined as [52]

$$M_n \triangleq \frac{E[r_o^n]}{r_{o,max}^n} = \frac{1}{(Ar_{max})^n} \int_0^\infty g^n(r) f_r(r) dr \tag{16}$$

where $f_r(r)$ is the probability density function (PDF) of signal envelope r . It follows that we can rewrite (15) as

$$\eta_{av,A} = \frac{1}{2} M_2(r_{max}), \eta_{av,B} = \frac{\pi}{4} \frac{M_2(r_{max})}{M_1(r_{max})}. \tag{17}$$

In this paper, we assume that the information signal and energy signal are a multi-carrier OFDM signal and multitone sine signal, respectively. When the subcarrier numbers are large enough, both signals can be approximated as complex Gaussian signals in the baseband. Thus, the composite signal can also be treated as a complex Gaussian signal. The PDF of its envelope is given by $(2r/P_{in}) / \exp(-r^2/P_{in})$. Given such a complex Gaussian signal approximation, the first and second non-central moments with the Saleh model are given by [53]

$$M_1(\xi) = 4\sqrt{\pi\xi} - 8\pi\xi \exp(4\xi) \operatorname{erfc}(2\sqrt{\xi}), \tag{18}$$

$$M_2(\xi) = 16\xi[(1 + 4\xi) \exp(4\xi) E_1(4\xi) - 1] \tag{19}$$

where $\operatorname{erfc}(x) = 1 - \operatorname{erf}(x)$ is the complementary error function and $E_n(x) = \int_1^\infty \frac{\exp(-xt)}{t^n} dt$ is the exponential integral.

For the polynomial model, substituting Equation (10) into Equation (16), the moments can be calculated as

$$M_1(\xi) = \left(\frac{\sqrt{\pi}}{2\sqrt{\xi}} + \frac{3c_1\sqrt{\pi}}{4\xi\sqrt{\xi}} + \frac{15c_2\sqrt{\pi\xi}}{8\xi^2} \right) \operatorname{erf}(\sqrt{\xi}) - \frac{6c_1 + 10c_2\xi + 15c_2}{4\xi \exp(\xi)}, \tag{20}$$

$$\begin{aligned}
 M_2(\zeta) = & \frac{(1 - \exp(-\zeta))}{\zeta} - \frac{4c_1(1 - (\zeta + 1)\exp(-\zeta))}{\zeta^2} \\
 & - \frac{(12c_2 + 6c_1^2 + 2c_2)(1 - (\zeta^2 + 2\zeta + 2)\exp(-\zeta))}{2\zeta^3} \\
 & - \frac{16c_1c_2}{\zeta^4} \left(3 - \frac{(\zeta^3 + 3\zeta^2 + 6\zeta + 6)\exp(-\zeta)}{2} \right) \\
 & - \frac{5c_2^2(1 - (\zeta^4 + 4\zeta^3 + 12\zeta^2 + 24\zeta + 24)\exp(-\zeta))}{\zeta^5}
 \end{aligned} \tag{21}$$

respectively.

We note that Equation (21) is associated with the specific polynomial model introduced in Equation (10). The coefficients in Equation (21) may change subject to different polynomial models.

4. SNDR Analysis

In the hybrid signaling SWIPT scenario, we have a mixture of a high-power energy signal and a low-power information signal. When the hybrid signal passes through nonlinear PAs [62], both signals will generate undesirable distortion signals that act as interference with the information signal. As a commonly used metric of signal distortion in communication systems, SNDR is broadly defined as the ratio of the useful signal to the total distortion power and noise power. The exact definitions of SNDR can take several forms, as proposed by C. Zhao [63], P. Zillmann [64], and R. Raich [65]. This paper adopts the definition in [65]. Considering an information transmission system, the output signal y of the PA can be written as the sum of two parts:

$$y = \alpha x + d. \tag{22}$$

The first item on the right-hand side is a linear amplification of the useful information signal, while the second item is the distortion signal, which is independent of x . The linear amplification factor α is defined as

$$\alpha = \frac{E[x^*y]}{E[|x|^2]}. \tag{23}$$

The power ϵ_d of the distortion term is defined as

$$\epsilon_d = E[|d|^2] = E[|y|^2] - |\alpha|^2 E[|x|^2]. \tag{24}$$

Given the above definitions, the SNDR can be defined as

$$\text{SNDR} = \frac{|\alpha|^2 E[|x|^2]}{\epsilon_d + \sigma_v^2} \tag{25}$$

where σ_v^2 is the noise power. Because the SWIPT signal consists of a large energy signal and a small information signal, the PA could have different linear amplification effects with respect to these two signals. When the effects of nonlinearity are not severe, the amplification coefficients of the two components can be approximately treated as the same. Otherwise, different amplification coefficients should be applied. For a comprehensive discussion, we further distinguish the following two cases of SNDR definitions.

4.1. Identical Amplification Coefficient

In this case, $y = \alpha(s + e) + d = \alpha x + d$. Because the energy signal and the information signal have an identical amplification factor, the definition of α is the same as that of the traditional SNDR defined in (23). Unlike the traditional SNDR definition, the power of the useful signal in SNDR definition should be expressed as the power of the information

signal. Therefore, according to Equation (25), the SNDR with respect to the information signal s can be obtained as

$$\text{SNDR} = \frac{|\alpha|^2 E[|s|^2]}{\epsilon_d + \sigma_v^2}. \tag{26}$$

Here, the linear coefficient α is a function of the signal envelope r , i.e.,

$$\alpha = \frac{\int_0^\infty r g(r) \exp(jf(r)) f_r(r) dr}{\int_0^\infty r^2 f_r(r) dr}. \tag{27}$$

where $f_r(r)$ denotes the PDF of signal envelope r . The power ϵ_d of the distortion term can be evaluated as

$$\epsilon_d = \int_0^\infty [g(r)]^2 f_r(r) dr - |\alpha|^2 \int_0^\infty r^2 f_r(r) dr. \tag{28}$$

4.2. Different Amplification Coefficients

In the case of different amplification coefficients, we have $y = \alpha s + \beta e + d$. The exact definitions of the two amplification coefficients α and β are given by

$$\alpha = \frac{E[s^*(y - \beta e)]}{E[|s|^2]}, \tag{29}$$

$$\beta = \frac{E[e^*(y - \alpha s)]}{E[|e|^2]}, \tag{30}$$

respectively. We can see that according to the above definitions, the two coefficients are mutually coupled and very difficult to calculate. Fortunately, in the SWIPT scenario, we can simplify the calculation with proper approximations. Exploiting the fact that the information signal s is small compared with the energy signal e , $y - \alpha s$ can be approximately treated as equal to y when we calculate β . It follows that we have $y \approx \beta e + d$. The amplification coefficient of the energy signal is then given by

$$\beta = \frac{E[e^* y]}{E[|e|^2]} \tag{31}$$

where

$$E[e^* y] = \int_0^\infty \int_0^\infty |e| g(r) \exp(j(\phi_x - \phi_e + f(r))) \cdot f_{ey}(e, y) dedy \tag{32}$$

and $f_{ey}(e, y)$ is the joint PDF of energy signal e and output signal y . Although function $f_{ey}(e, y)$ cannot be expressed in closed form, it can be numerically evaluated.

The power of the distortion term can be written as

$$\epsilon_d = E[|d|^2] = E[|y|^2] - |\alpha|^2 E[|s|^2] - |\beta|^2 E[|e|^2]. \tag{33}$$

Finally, the SNDR can be expressed as

$$\text{SNDR} = \frac{|\alpha|^2 E[|s|^2]}{\epsilon_d + \sigma_v^2} = \frac{|\alpha|^2 E[|s|^2]}{E[|y|^2] - |\alpha|^2 E[|s|^2] - |\beta|^2 E[|e|^2] + \sigma_v^2}. \tag{34}$$

5. Numerical Results and Discussion

This section presents numerical results based on the above analysis. The default values of parameters used in this section are set as follows. The maximum amplitude of linear amplification r_{\max} is set to be 3, the ideal amplification gain coefficient of PA A is 10, the effective IBO ranges from -5 dB to 15 dB. The power of the information signal is

set to be constant, the power ratio of the energy signal to the information signal P_E/P_I ranges from 4 to 256, and the noise power σ_v^2 is set to -100 dB. Complex Gaussian signals are used to approximate the multi-carrier information signal and multitone energy signal. In some figures, theoretical results and simulation results are presented for comparison purposes. The theoretical results are obtained from numerical computation of closed-form or semi-closed-form equations, while the simulation results are obtained from Monte Carlo simulations and sample-based numerical evaluation. The presented results are statistically averaged over 50 trials.

Figure 5 compares the PA efficiency of Class A and Class B PAs as a function of the effective IBO. Results for both the Saleh model and polynomial model are shown. The theoretical and simulation results are calculated based on Equations (17) and (15), respectively, which are shown to agree well. As expected, the efficiency of PA generally decreases with the increase in IBO. The efficiency of Class B exceeds that of Class A, with a gain ranging from 10 dB to 40 dB. The efficiency differences are more significant at smaller values of IBO. Moreover, the efficiency given by the polynomial model is slightly better than that of the Saleh model. This is because the polynomial model exhibits a slightly higher AM-AM curve, as shown in Figure 4. Such difference diminishes with increasing IBO. Figure 5 successfully establishes the relationship between PA efficiency and IBO. The next step is to link IBO with SNDR, such that we can use IBO as an intermediate parameter to characterize the tradeoff between PA efficiency and SNDR.

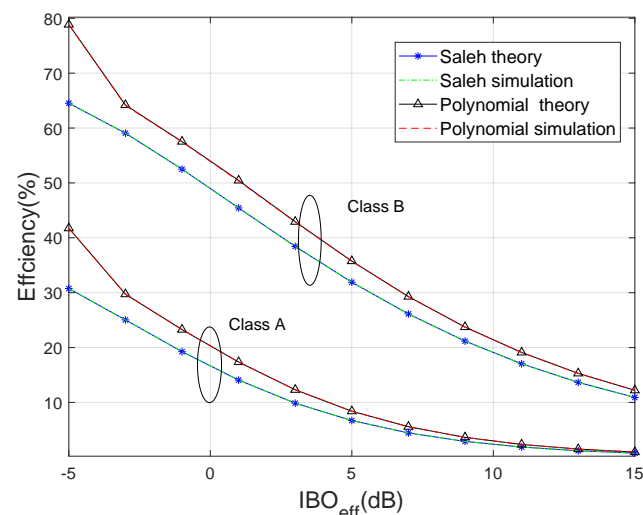


Figure 5. The efficiency of Class A and Class B PAs as a function of the effective IBO (Class A and Class B PAs, Saleh, and polynomial models).

Figure 6 shows the relationship between effective IBO and SNDR under different energy-to-information signal power ratios. Results are shown for the two different cases discussed in Section 4. Case I refers to the case where we have the same amplification coefficients, while Case II denotes the case with different coefficients. For Case I, we can have both theoretical and simulation results based on the equations presented in Section 4.1. For Case II, we can only have simulation results based on Equation (34). For notation simplicity, the SNDR values obtained by Case I theory, Case I simulation, and Case II simulation are denoted as I(1), I(2), and II(2) in the figure legend, respectively.

In Figure 6, SNDR values are shown to increase almost linearly with increasing IBO (both in dB values). The SNDR difference between Case I and Case II is not very significant, only reaching a maximum value of 2 dB when the IBO is 15 dB. Moreover, the SNDR given by the polynomial model is slightly better than the Saleh model. This is because the memoryless polynomial model in (9) assumes no AM-PM distortion. Another finding presented in Figure 6 is that the SNDR decreases with increasing P_E/P_I power ratio. This

is expected because a higher-power energy signal will generate more interference with the information signal. Figure 6 establishes the relationship between SNDR and IBO.

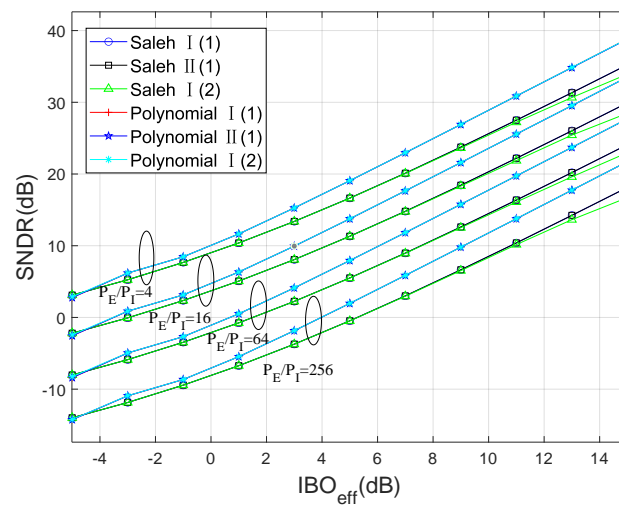


Figure 6. The SNDR as a function of the effective IBO with varying power ratios (Class B PA, Saleh, and polynomial models).

Building on the results shown in Figures 5–7 show the tradeoff between SNDR and PA efficiency with different PA classes and different PA models. The power ratio is fixed at 64. We can see that, given a targeted SNDR value, the two PA classes contribute to the most significant efficiency difference at around 20 dB. The two different PA models also lead to a small difference of less than 5 dB. The two different cases of SNDR definition give almost identical curves. A slightly concave-shaped tradeoff relationship is observed for SNDR and efficiency.

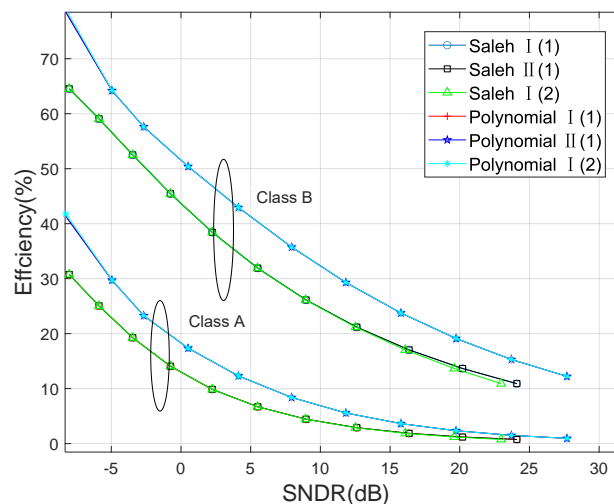


Figure 7. The tradeoff relationship between SNDR and PA efficiency ($P_E/P_I = 64$, Class A and Class B PAs, Saleh, and polynomial models).

Similar to Figure 7, Figure 8 shows the relationship between SNDR and PA efficiency with different power ratios. We can see that increasing the power ratio in an exponential fashion has a similar effect as shifting the tradeoff curve horizontally towards the left-hand side along the X-axis. This implies a negative linear relationship between the power ratio (in dB) and the SNDR. Again, the differences caused by using the Saleh and polynomial models are limited to 5 dB.

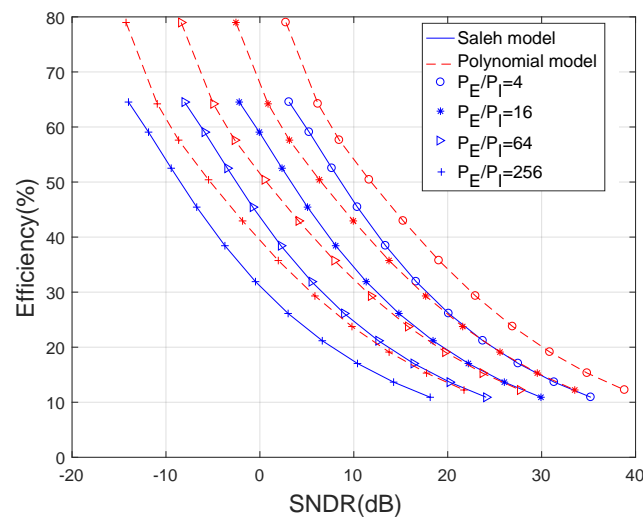


Figure 8. The tradeoff relationship between SNDR and PA efficiency with varying power ratios (Class B PA, Case I(1), Saleh, and polynomial models).

To pinpoint the results more accurately, Table 1 shows the efficiency of different PAs with different values of SNDR and power ratios. We can see that as the energy-to-information signal power ratio increases, the corresponding SNDR under the same efficiency is significantly reduced.

Table 1. Efficiency of different PAs with different values of SNDR and power ratios.

Power Ratio	Class A				Class B						
	Saleh PA		Polynomial PA		Saleh PA			Polynomial PA			
	SNDR (dB)										
	10	20	10	20	10	20	30	10	20	30	
4	14.4	4.5	20.7	8.1	45.9	26.1	14.2	54.3	34.8	20.1	
16	7.8	2.4	12.3	4.7	35.1	19.4	10.9	42.9	26.6	15.1	
64	4.2	1.2	6.8	2.3	24.9	13.6	-	32.5	18.9	-	
256	1.9	-	3.6	1.0	17.1	-	-	23.7	13.8	-	

In the literature of nonlinear PA analysis, it is a common practice to measure the nonlinear distortion effect by observing the power spectral density (PSD) of signals after a nonlinear PA. In the frequency domain, nonlinear distortion is manifested as power leakage into the adjacent bands. The adjacent channel power ratio (ACPR) is defined as the ratio of the signal power at the central frequency versus the power at an adjacent frequency (i.e., frequency offset). Similar to SNDR, ACPR is also a metric for nonlinear distortion. Figure 9 aims to show the correlation between these two commonly used metrics. A simulation is performed to measure the ACPR and SNDR. The information signal is taken as an OFDM signal with a bandwidth of 5 MHz, while the energy signal is a multitone sine signal. In Figure 9, when the SNDR is measured to be 10 dB, 20 dB, and 30 dB, the corresponding ACPR values at the 5 MHz offset are roughly -25 dB, -34 dB, and -41 dB, respectively. This means that the variations in the theoretically calculated SNDR are mirrored by ACPR in the simulations. This further validates the practical value of the SNDR metrics.

From the above discussion, we can see that maximizing SNDR and PA efficiency represents two conflicting objectives in a SWIPT system. The performance of a hybrid signaling SWIPT system is fundamentally characterized by the tradeoff relationship between SNDR and PA efficiency. In practice, an appropriate SNDR efficiency operational point should be carefully chosen for a targeted application.

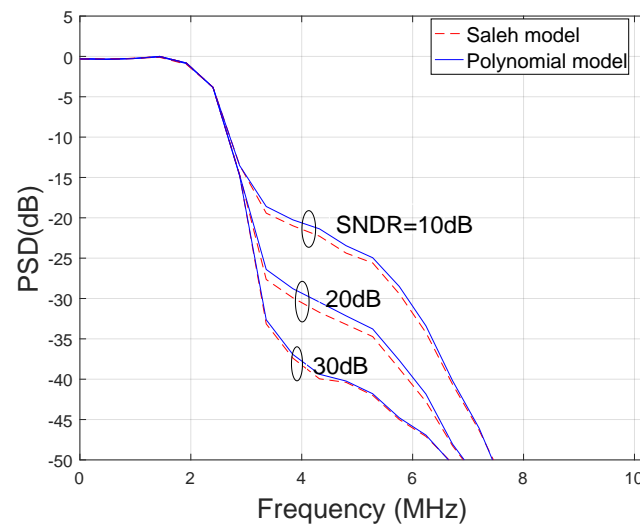


Figure 9. Power spectral density (PSD) of the information signal after nonlinear PA. In the simulation, we select the OFDM signal with the bandwidth of 5 MHz as the information signal and the multitone sine signal as the energy signal, and we create the power spectral density images of the information signal after PA of Class B when the given SNDR of $I(1)$ is 10 dB, 20 dB, 30 dB.

6. Conclusions

This paper presents a systematic analysis of the performance of hybrid signaling SWIPT systems with nonlinear PAs. Using PA efficiency and SNDR as performance metrics, we have presented a quantitative analysis of the conflicting design objectives in SWIPT. Our study has taken into account the variations in PA types, PA models, and SNDR metrics. Theoretical and simulation results have revealed a concave-shaped tradeoff relationship between the SNDR and PA efficiency. Furthermore, a nearly linear relationship has been revealed between the energy-to-information signal power ratio (in dB) and the SNDR. It has been shown that, for the SNDR value, the PA efficiency differences between Class A and Class B PAs are around 20dB. Our study reveals a fundamental tradeoff in SWIPT systems and provides useful guidelines for the design of practical SWIPT systems with hybrid signaling schemes.

Author Contributions: Conceptualization, X.W. (Xiaofang Wu); methodology, X.W. (Xiaofang Wu); software, L.C.; validation, X.W. (Xiaofang Wu), L.C. and X.W. (Xin Wang); formal analysis, X.W. (Xiaofang Wu) and L.C.; investigation, L.C.; resources, L.C.; data curation, X.W. (Xin Wang); writing—original draft preparation, W.Q.; writing—review and editing, L.C.; visualization, X.H.; supervision, J.S.; project administration, J.H.; funding acquisition, K.Y. All authors have read and agreed to the published version of the manuscript.

Funding: This research was funded by the National Natural Science Foundation of China (Grant No. U1705263) and the Science and Technology Key Project of Fujian Province, China (No. 2019HZ020009).

Acknowledgments: We express our thanks to the editors and anonymous reviewers for their valuable comments.

Conflicts of Interest: The authors declare no conflict of interest.

Appendix A

According to Figure 4, the AM-AM characteristics of the nonlinear PA are as follows: as $\frac{r}{r_{\max}}$ increases, $\frac{r_o}{r_{o,\max}}$ changes from a rapid increase to a slow increase, and even after a certain value begins to fall, the maximum value does not exceed one. We can then substitute $g(r)$ of the polynomial model into Equation (10). When $\frac{r}{r_{\max}}$ is $0 \rightarrow 1$, the $g(r)$ curve tends to be flat—that is, $g'(1) < g'(0)$. Let r_1 be the maximum point of $g(r)$, then

$g'(r_1) = 0$. At this time, $\frac{r_1}{r_{\max}} > 1$, $\frac{g(r_1)}{r_{o,\max}} \leq 1$. We take up $\frac{r_1}{r_{\max}} = 2$ as the maximum value point and calculate the coefficient value that satisfies the above constraints; then, we obtain $c_1 = -\frac{3}{16}$, $c_2 = \frac{1}{64}$.

References

1. Yang, Z.; Chen, M.; Wong, K.K.; Poor, H.V.; Cui, S. Federated Learning for 6G: Applications, Challenges, and Opportunities. *arXiv* **2021**, arXiv:2101.01338.
2. Hu, J.; Li, M.; Yang, K.; Ng, S.X.; Wong, K.K. Unary coding controlled simultaneous wireless information and power transfer. *IEEE Trans. Wirel. Commun.* **2019**, *19*, 637–649. [[CrossRef](#)]
3. Li, A.; Masouros, C. Energy-efficient SWIPT: From fully digital to hybrid analog–digital beamforming. *IEEE Trans. Veh. Technol.* **2017**, *67*, 3390–3405. [[CrossRef](#)]
4. Choi, B.H.; Thai, V.X.; Lee, E.S.; Kim, J.H.; Rim, C.T. Dipole-coil-based wide-range inductive power transfer systems for wireless sensors. *IEEE Trans. Ind. Electron.* **2016**, *63*, 3158–3167. [[CrossRef](#)]
5. Atallah, R.F.; Assi, C.M.; Yu, J.Y. A reinforcement learning technique for optimizing downlink scheduling in an energy-limited vehicular network. *IEEE Trans. Veh. Technol.* **2016**, *66*, 4592–4601. [[CrossRef](#)]
6. Hu, J.; Yang, K.; Wen, G.; Hanzo, L. Integrated data and energy communication network: A comprehensive survey. *IEEE Commun. Surv. Tutor.* **2018**, *20*, 3169–3219. [[CrossRef](#)]
7. Varshney, L.R. Transporting information and energy simultaneously. In Proceedings of the 2008 IEEE International Symposium on Information Theory, Toronto, ON, Canada, 6–11 July 2008; pp. 1612–1616.
8. Huang, G.; Zhang, Q.; Qin, J. Joint time switching and power allocation for multicarrier decode-and-forward relay networks with SWIPT. *IEEE Signal Process. Lett.* **2015**, *22*, 2284–2288. [[CrossRef](#)]
9. Dong, Y.; Hossain, M.J.; Cheng, J. Joint power control and time switching for SWIPT systems with heterogeneous QoS requirements. *IEEE Commun. Lett.* **2015**, *20*, 328–331. [[CrossRef](#)]
10. Krikidis, I.; Timotheou, S.; Nikolaou, S.; Zheng, G.; Ng, D.W.K.; Schober, R. Simultaneous wireless information and power transfer in modern communication systems. *IEEE Commun. Mag.* **2014**, *52*, 104–110. [[CrossRef](#)]
11. Zhou, X. Training-based SWIPT: Optimal power splitting at the receiver. *IEEE Trans. Veh. Technol.* **2014**, *64*, 4377–4382. [[CrossRef](#)]
12. Ding, Z.; Perlaza, S.M.; Esnaola, I.; Poor, H.V. Power allocation strategies in energy harvesting wireless cooperative networks. *IEEE Trans. Wirel. Commun.* **2014**, *13*, 846–860. [[CrossRef](#)]
13. Chen, H.; Li, Y.; Jiang, Y.; Ma, Y.; Vucetic, B. Distributed power splitting for SWIPT in relay interference channels using game theory. *IEEE Trans. Wirel. Commun.* **2014**, *14*, 410–420. [[CrossRef](#)]
14. Abedi, M.; Masoumi, H.; Emadi, M.J. Power splitting-based SWIPT systems with decoding cost. *IEEE Wirel. Commun. Lett.* **2018**, *8*, 432–435. [[CrossRef](#)]
15. Guo, S.; Zhang, H.; Wang, Y.; Yuan, D. Spatial modulated simultaneous wireless information and power transfer. In Proceedings of the 2016 IEEE Global Communications Conference (GLOBECOM), Washington, DC, USA, 4–8 December 2016; pp. 1–6.
16. Koo, B.; Park, D. Interference alignment and wireless energy transfer via antenna selection. *IEEE Commun. Lett.* **2014**, *18*, 548–551. [[CrossRef](#)]
17. Zhao, S.; Li, Q.; Zhang, Q.; Qin, J. Antenna selection for simultaneous wireless information and power transfer in MIMO systems. *IEEE Commun. Lett.* **2014**, *18*, 789–792. [[CrossRef](#)]
18. Jang, H.H.; Choi, K.W.; Kim, D.I. Novel frequency-splitting SWIPT for overcoming amplifier nonlinearity. *IEEE Wirel. Commun. Lett.* **2020**, *9*, 826–829. [[CrossRef](#)]
19. Clerckx, B.; Zhang, R.; Schober, R.; Ng, D.W.K.; Kim, D.I.; Poor, H.V. Fundamentals of Wireless Information and Power Transfer: From RF Energy Harvester Models to Signal and System Designs. *IEEE J. Sel. Areas Commun.* **2019**, *37*, 4–33. [[CrossRef](#)]
20. Boshkovska, E.; Ng, D.W.K.; Zlatanov, N.; Schober, R. Practical Non-Linear Energy Harvesting Model and Resource Allocation for SWIPT Systems. *IEEE Commun. Lett.* **2015**, *19*, 2082–2085. [[CrossRef](#)]
21. Guerreiro, J.; Dinis, R.; Montezuma, P. On the Assessment of Nonlinear Distortion Effects in MIMO-OFDM Systems. In Proceedings of the IEEE 83rd Vehicular Technology Conference (VTC Spring), Nanjing, China, 15–18 May 2016; pp. 1–5.
22. Ozel, O.; Ulukus, S. Achieving AWGN capacity under stochastic energy harvesting. *IEEE Trans. Inf. Theory* **2012**, *58*, 6471–6483. [[CrossRef](#)]
23. Ozel, O.; Ulukus, S. AWGN channel under time-varying amplitude constraints with causal information at the transmitter. In Proceedings of the 2011 Conference Record of the Forty Fifth Asilomar Conference on Signals, Systems and Computers (ASILOMAR), Pacific Grove, CA, USA, 6–9 November 2011; pp. 373–377.
24. Tutuncuoglu, K.; Ozel, O.; Yener, A.; Ulukus, S. Binary energy harvesting channel with finite energy storage. In Proceedings of the 2013 IEEE International Symposium on Information Theory, Istanbul, Turkey, 7–12 July 2013; pp. 1591–1595.
25. Xiong, K.; Wang, B.; Liu, K.R. Rate-energy region of SWIPT for MIMO broadcasting under nonlinear energy harvesting model. *IEEE Trans. Wirel. Commun.* **2017**, *16*, 5147–5161. [[CrossRef](#)]
26. Niu, H.; Guo, D.; Huang, Y.; Zhang, B. Robust energy efficiency optimization for secure MIMO SWIPT systems with non-linear EH model. *IEEE Commun. Lett.* **2017**, *21*, 2610–2613. [[CrossRef](#)]

27. Zhang, R.; Ho, C.K. MIMO broadcasting for simultaneous wireless information and power transfer. *IEEE Trans. Wirel. Commun.* **2013**, *12*, 1989–2001. [[CrossRef](#)]
28. Hu, Z.; Yuan, C.; Gao, F. Maximizing harvested energy for full-duplex SWIPT system with power splitting. *IEEE Access* **2017**, *5*, 24975–24987. [[CrossRef](#)]
29. Jiang, R.; Xiong, K.; Fan, P.; Zhang, Y.; Zhong, Z. Optimal design of SWIPT systems with multiple heterogeneous users under non-linear energy harvesting model. *IEEE Access* **2017**, *5*, 11479–11489. [[CrossRef](#)]
30. Zhou, X.; Zhang, R.; Ho, C.K. Wireless information and power transfer: Architecture design and rate-energy tradeoff. *IEEE Trans. Commun.* **2013**, *61*, 4754–4767. [[CrossRef](#)]
31. Zhao, Y.; Hu, J.; Ding, Z.; Yang, K. Joint interleaver and modulation design for multi-user SWIPT-NOMA. *IEEE Trans. Commun.* **2019**, *67*, 7288–7301. [[CrossRef](#)]
32. Perera, T.D.P.; Jayakody, D.N.K.; Sharma, S.K.; Chatzinotas, S.; Li, J. Simultaneous wireless information and power transfer (SWIPT): Recent advances and future challenges. *IEEE Commun. Surv. Tutor.* **2017**, *20*, 264–302. [[CrossRef](#)]
33. Pan, C.; Ren, H.; Wang, K.; Elkashlan, M.; Nallanathan, A.; Wang, J.; Hanzo, L. Intelligent Reflecting Surface Aided MIMO Broadcasting for Simultaneous Wireless Information and Power Transfer. *IEEE J. Sel. Areas Commun.* **2020**, *38*, 1719–1734. [[CrossRef](#)]
34. Bai, T.; Pan, C.; Ren, H.; Deng, Y.; Elkashlan, M.; Nallanathan, A. Resource Allocation for Intelligent Reflecting Surface Aided Wireless Powered Mobile Edge Computing in OFDM Systems. *IEEE Trans. Wireless Commun.* **2021**. [[CrossRef](#)]
35. Pan, Y.; Wang, K.; Pan, C.; Zhu, H.; Wang, J. Self-Sustainable Reconfigurable Intelligent Surface Aided Simultaneous Terahertz Information and Power Transfer (STIPT). *arXiv* **2021**, arXiv:2102.04053.
36. Ni, R.; Mayaram, K.; Fiez, T.S. A 915 MHz, 6 Mb/s, 80 pJ/b BFSK receiver with- 76dBm sensitivity for high data rate wireless sensor networks. In Proceedings of the 2014 Symposium on VLSI Circuits Digest of Technical Papers, Honolulu, HI, USA, 10–13 June 2014; pp. 1–2.
37. Chatterjee, S.; Tarique, M. A 100-nW sensitive RF-to-DC CMOS rectifier for energy harvesting applications. In Proceedings of the 2016 29th International Conference on VLSI Design and 2016 15th International Conference on Embedded Systems (VLSID), Kolkata, India, 4–8 January 2016; pp. 557–558.
38. Clerckx, B. Wireless information and power transfer: Nonlinearity, waveform design, and rate-energy tradeoff. *IEEE Trans. Signal Process.* **2017**, *66*, 847–862. [[CrossRef](#)]
39. Claessens, S.; Chang, Y.T.; Schreurs, D.; Pollin, S. Receiving ASK-OFDM in Low Power SWIPT Nodes without Local Oscillators. In Proceedings of the 2019 IEEE Wireless Power Transfer Conference (WPTC), London, UK, 18–21 June 2019; pp. 20–25.
40. Collado, A.; Georgiadis, A. Optimal waveforms for efficient wireless power transmission. *IEEE Microw. Wirel. Components Lett.* **2014**, *24*, 354–356. [[CrossRef](#)]
41. Claessens, S.; Rajabi, M.; Pan, N.; Pollin, S.; Schreurs, D. Measurement-based analysis of the throughput-power level trade-off with modulated multisine signals in a SWIPT system. In Proceedings of the 2017 89th ARFTG Microwave Measurement Conference (ARFTG), Honolulu, HI, USA, 9 June 2017; pp. 1–4.
42. Clerckx, B.; Bayguzina, E. Waveform design for wireless power transfer. *IEEE Trans. Signal Process.* **2016**, *64*, 6313–6328. [[CrossRef](#)]
43. Ikeuchi, T.; Kawahara, Y. Signal Detection Method Based on Peak to Average Ratio for Frequency Shift Multitone SWIPT System. In Proceedings of the 2020 IEEE Wireless Power Transfer Conference (WPTC), Seoul, Korea, 15–19 November 2020; pp. 119–122.
44. Lu, Y.; Xiong, K.; Fan, P.; Zhong, Z.; Letaief, K.B. Robust transmit beamforming with artificial redundant signals for secure SWIPT system under non-linear EH model. *IEEE Trans. Wirel. Commun.* **2018**, *17*, 2218–2232. [[CrossRef](#)]
45. Huang, X.; Li, Q.; Zhang, Q.; Qin, J. Power allocation for secure OFDMA systems with wireless information and power transfer. *Electron. Lett.* **2014**, *50*, 229–230. [[CrossRef](#)]
46. Kim, I.M.; Kim, D.I.; Kang, J.M. Rate-energy tradeoff and decoding error probability-energy tradeoff for SWIPT in finite code length. *IEEE Trans. Wirel. Commun.* **2017**, *16*, 8220–8234. [[CrossRef](#)]
47. Yang, Z.; Xu, W.; Pan, Y.; Pan, C.; Chen, M. Energy Efficient Resource Allocation in Machine-to-Machine Communications With Multiple Access and Energy Harvesting for IoT. *IEEE Internet Things J.* **2018**, *5*, 229–245. [[CrossRef](#)]
48. Ma, W.; Li, C.; Quan, X.; Pan, W.; Xu, Q.; Liu, Y.; Tang, Y. A Nonlinear Feedback Linearized Power Amplifier for Wireless Communication Systems. In Proceedings of the 2018 IEEE International Symposium on Signal Processing and Information Technology (ISSPIT), Louisville, KY, USA, 6–8 December 2018; pp. 241–246.
49. Iofedov, I.; Wulich, D. MIMO-OFDM with nonlinear power amplifiers. *IEEE Trans. Commun.* **2015**, *63*, 4894–4904. [[CrossRef](#)]
50. Kim, J.; Clerckx, B.; Mitcheson, P.D. Experimental analysis of harvested energy and throughput trade-off in a realistic SWIPT system. In Proceedings of the 2019 IEEE Wireless Power Transfer Conference (WPTC), London, UK, 18–21 June 2019; pp. 1–5.
51. Lavrador, P.M.; de Carvalho, N.B.; Pedro, J.C. Evaluation of signal-to-noise and distortion ratio degradation in nonlinear systems. *IEEE Trans. Microw. Theory Tech.* **2004**, *52*, 813–822. [[CrossRef](#)]
52. Raab, F.H.; Asbeck, P.; Cripps, S.; Kerington, P.B.; Popovic, Z.B.; Potheary, N.; Sevic, J.F.; Sokal, N.O. Power amplifiers and transmitters for RF and microwave. *IEEE Trans. Microw. Theory Tech.* **2002**, *50*, 814–826. [[CrossRef](#)]
53. Ochiai, H. An analysis of band-limited communication systems from amplifier efficiency and distortion perspective. *IEEE Trans. Commun.* **2013**, *61*, 1460–1472. [[CrossRef](#)]
54. Saleh, A.A.; Salz, J. Adaptive linearization of power amplifiers in digital radio systems. *Bell Syst. Tech. J.* **1983**, *62*, 1019–1033. [[CrossRef](#)]

55. Joung, J.; Ho, C.K.; Adachi, K.; Sun, S. A survey on power-amplifier-centric techniques for spectrum-and energy-efficient wireless communications. *IEEE Commun. Surv. Tutor.* **2014**, *17*, 315–333. [[CrossRef](#)]
56. Vuolevi, J.H.; Rahkonen, T.; Manninen, J.P. Measurement technique for characterizing memory effects in RF power amplifiers. *IEEE Trans. Microw. Theory Tech.* **2001**, *49*, 1383–1389. [[CrossRef](#)]
57. Golestaneh, H.; Abdipour, A.; Mohammadi, A. Nonlinear modeling and analysis of a Doherty power amplifier driven by non-constant envelope signals. *Analog Integr. Circuits Signal Process.* **2012**, *72*, 141–153. [[CrossRef](#)]
58. Taghian, F.; Abdipour, A.; Mohammadi, A.; Roodaki, P.M. Design and nonlinear analysis of a dual-band Doherty power amplifier for ISM and LMDS applications. In Proceedings of the 2011 IEEE Applied Electromagnetics Conference (AEMC), Kolkata, India, 18–22 December 2011; pp. 1–4.
59. Wang, F.; Yang, A.H.; Kimball, D.F.; Larson, L.E.; Asbeck, P.M. Design of wide-bandwidth envelope-tracking power amplifiers for OFDM applications. *IEEE Trans. Microw. Theory Tech.* **2005**, *53*, 1244–1255. [[CrossRef](#)]
60. Yang, Y.; Cha, J.; Shin, B.; Kim, B. A microwave Doherty amplifier employing envelope tracking technique for high efficiency and linearity. *IEEE Microw. Wirel. Components Lett.* **2003**, *13*, 370–372. [[CrossRef](#)]
61. Wulich, D. Definition of efficient PAPR in OFDM. *IEEE Commun. Lett.* **2005**, *9*, 832–834. [[CrossRef](#)]
62. Bassam, S.A.; Helaoui, M.; Ghannouchi, F.M. 2-D Digital Predistortion (2-D-DPD) Architecture for Concurrent Dual-Band Transmitters. *IEEE Trans. Microw. Theory Tech.* **2011**, *59*, 2547–2553. [[CrossRef](#)]
63. Zhao, C.; Baxley, R.J.; Zhou, G.T. SNDR Analysis for Transceiver Nonlinearities in AWGN Channels. In Proceedings of the 2007 IEEE/SP 14th Workshop on Statistical Signal Processing, Madison, WI, USA, 26–29 August 2007; pp. 522–526.
64. Zillmann, P. Relationship between Two Distortion Measures for Memoryless Nonlinear Systems. *IEEE Signal Process. Lett.* **2010**, *17*, 917–920. [[CrossRef](#)]
65. Qian, H.; Raich, R.; Zhou, G. Optimization of SNDR in the presence of amplitude limited nonlinearity and multipath fading. In Proceedings of the Conference Record of the Thirty-Eighth Asilomar Conference on Signals, Systems and Computers, Pacific Grove, CA, USA, 7–10 November 2004; Volume 1, pp. 712–716.